

BEING WISE I: VALIDATING STELLAR POPULATION MODELS AND M_*/L RATIOS AT 3.4 AND $4.6\mu\text{m}$

MARK A. NORRIS¹, SHARON MEIDT¹, GLENN VAN DE VEN¹, EVA SCHINNERER¹, BRENT GROVES¹ & MIGUEL QUEREJETA¹

(Dated: July 24, 2014)
 Draft version July 24, 2014

ABSTRACT

Using data from the WISE mission, we have measured near infra-red (NIR) photometry of a diverse sample of dust-free stellar systems (globular clusters, dwarf and giant early-type galaxies) which have metallicities that span the range $-2.2 < [\text{Fe}/\text{H}] \text{ (dex)} < 0.3$. This dramatically increases the sample size and broadens the metallicity regime over which the 3.4 (W1) and $4.6\mu\text{m}$ (W2) photometry of stellar populations have been examined.

We find that the W1 - W2 colors of intermediate and old (> 2 Gyr) stellar populations are insensitive to the age of the stellar population, but that the W1 - W2 colors become bluer with increasing metallicity, a trend not well reproduced by most stellar population synthesis (SPS) models. In common with previous studies, we attribute this behavior to the increasing strength of the CO absorption feature located in the $4.6\mu\text{m}$ bandpass with metallicity.

Having used our sample to validate the efficacy of some of the SPS models, we use these models to derive stellar mass-to-light ratios in the W1 and W2 bands. Utilizing observational data from the SAURON and ATLAS3D surveys, we demonstrate that these bands provide extremely simple, yet robust stellar mass tracers for dust free older stellar populations that are freed from many of the uncertainties common among optical estimators.

1. INTRODUCTION

Stellar population synthesis models are an important tool to investigate the formation and evolution of galaxies. By comparison of SPS models with observed galaxy spectral energy distributions (SEDs) it is possible to infer the mass of stars, gas, and dust, as well as the age and chemical enrichment of the underlying stellar populations (see e.g. Walcher et al. 2011; Conroy 2013).

Much recent work has focussed on the development of SPS models that accurately describe the behavior of galaxies in the near-to-mid infrared (e.g. da Cunha et al. 2008; Marigo et al. 2008; Kotulla et al. 2009; Conroy et al. 2009a; Bressan et al. 2012, 2013). In part because the near infrared bands are thought to be a more accurate proxy for total stellar mass than optical regions, due to the reduced importance of dust attenuation or short-lived but luminous young stars in IR bands. Importantly, however, dust *emission* can significantly effect the NIR colors of stellar systems (Meidt et al. 2012; Peletier et al. 2012; Querejeta et al. 2014) and must therefore be carefully taken into account when using NIR photometry as a stellar mass tracer. Yet, despite the rapid increase in theoretical predictions for the behavior of galaxy SEDs in the near and mid IR, to date only a limited number of studies have calibrated these predictions to observations of real stellar systems.

Spitler et al. (2008) compared the predictions of a range of Single Stellar Population (SSP) models to the optical - *Spitzer* IRAC [3.6] colors of a sample of globular clusters (GCs) from the Sombbrero and Centaurus A galaxies. They found generally good agreement in the colors, though with some evidence that the models could be under predicting the [3.6] flux at lower metallicities.

Peletier et al. (2012) then investigated the behavior of the *Spitzer* IRAC [3.6] - [4.5] color of the SAURON sample of early-type galaxies (de Zeeuw et al. 2002). They concluded that the galaxies displayed a color trend with metallicity over the limited metallicity range that they probed ($[\text{Fe}/\text{H}] > -0.5$). The sense of this trend was reversed relative to that observed in the optical (i.e. that in this case increasing metallicity led to bluer colors), and was not well reproduced by SPS models except for ones which included the influence of a strong CO absorption band in the [4.5] filter whose strength is temperature dependent.

Subsequently Barmby & Jalilian (2012) compared SSP models to V band and *Spitzer* IRAC photometry of bright globular clusters (GCs) from M31 also finding that the models examined were systematically redder than the data at higher metallicity.

Each of these previous studies suffered from either limited wavelength coverage in the NIR (Spitler et al. 2008), restricted metallicity range of the sample studied (Peletier et al. 2012), or limited statistical power due to a small sample size (Barmby & Jalilian 2012), or some combination of all three.

In light of these results and the recent explosion in the amount of galaxy photometry available in the NIR, provided by both large surveys using the *Spitzer* Space Telescope (e.g. S⁴G; Sheth et al. 2010) and the all sky coverage of the WISE mission (Wright et al. 2010), we have revisited the behavior of stellar populations in the NIR. We do this by analyzing a comprehensive sample of globular clusters and early-type galaxies in order to probe the color-metallicity behavior over a very wide metallicity range. We focus on GCs and early-type galaxies because these systems are essentially dust-free (e.g. Barmby et al. 2009; di Serego Alighieri et al. 2013), and as described previously dust emission can significantly alter the NIR colors of stellar systems.

norris@mpia.de

¹ Max Planck Institut für Astronomie, Königstuhl 17, D-69117, Heidelberg, Germany

Our work is further motivated by recent work by Meidt et al. (2014) who demonstrated that the $[3.6] - [4.5]$ color can be used to improve the estimation of $3.6\mu\text{m}$ stellar mass-to-light ratio. To do this they empirically derived a relation between the J-K and $[3.6] - [4.5]$ colors of giant stars, thereby avoiding the uncertainties present in the SPS models due to incorrect molecular line opacities of the template stars in the NIR. In doing this they provided a significantly improved stellar mass estimator than available at shorter wavelengths. However, the empirical relation needs to be verified for complex stellar populations over the age and metallicity ranges where it is likely to be used.

2. DATA ANALYSIS

For each of our samples being considered (see Section 4), except for the globular clusters of M31 which are essentially unresolved in WISE imaging, we downloaded and analysed the full (i.e. not thumbnail) ALLWISE² Atlas images. These images have been pipeline processed as described in Wright et al. (2010) and Mainzer et al. (2011) to produce co-added image tiles with uniform zeropoint that are spatially co-aligned in all four WISE bands. They are the result of co-adding all available WISE imaging, including NEOWISE imaging not previously included in earlier data releases, hence they represent the deepest WISE imaging available to date.

We choose to analyse WISE imaging (as opposed to Spitzer IRAC imaging) of our old stellar systems for a number of reasons; 1) WISE has consistent all-sky coverage ensuring large sample sizes. 2) The survey is relatively deep, with at least $S/N = 5$ for $W1 = 16.9$ and $W2 = 16.0$ mag, approximately twice as deep as 2MASS. 3) The large ($1.56^\circ \times 1.56^\circ$) field-of-view of the processed atlas images reduces sky subtraction problems for large apparent size objects such as Milky Way (MW) GCs and nearby massive early-type galaxies which often have half-light radii $> 3'$. 4) The resolution of the W1 and W2 bands while low by optical standards ($\sim 8.5''$ sampled with $1.375''$ pixels) is more than adequate to study nearby GCs and galaxies.

2.1. Stochastic Effects

When studying the integrated properties of lower mass stellar populations such as globular clusters it is necessary to consider to what degree measured quantities depend on the stochastic population of rare but luminous stellar phases, such as the red giant or asymptotic giant branches. The random appearance of a small number of stars on these evolved branches can lead to dramatic changes in both the total luminosity of the stellar population, and its color (see e.g. Fouesneau & Lançon 2010; Popescu & Hanson 2010). Especially in the optical where the colors of extreme red giant branch stars and the turnoff stars can differ by as much as a magnitude.

In contrast to the usual approach of theoretically determining the minimum stellar mass required to reduce stochastic population effects to manageable levels (see e.g. Barmby & Jalilian 2012) we choose to use an empirical procedure to determine the necessary stellar mass to limit the effect of stochastic population of the evolved

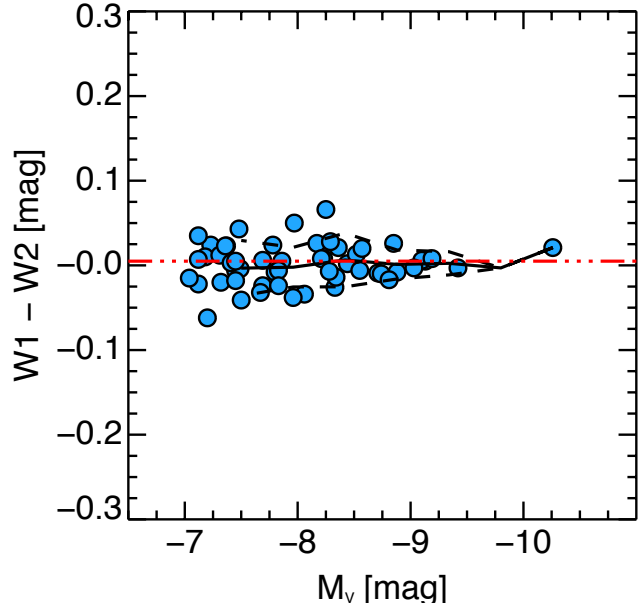


Figure 1. W1-W2 color measured within R_e for Milky Way globular clusters as a function of total V-band absolute magnitude. The solid black line shows the running average and the dashed lines the scatter. The red triple-dot-dashed line show the median W1 - W2 color of all GCs where the error in the W1 - W2 color is less than 0.05 mag.

phases on the measured color. To do this we have measured the W1-W2 color within the half-light-radius for all suitable MW GCs with $M_V < -7$ (corresponding to total luminosities sampled of 0.75 mag less due to our approach of only sampling to one effective radius).

As shown in Figure 1 the magnitude dependence of the scatter of the measured W1 - W2 colors is remarkably small, with very little dependence on total magnitude of the cluster other than that expected from purely photometric errors. This result is unexpected given that the scatter in this plot is composed of three effects; 1) photometric uncertainties, 2) the effect of the metallicity dependence of the color, and 3) the effect of stochastically populating the evolved branches. Therefore, given the observed low scatter, the known photometric errors (of around 0.01 mag for Milky Way GCs), and expected color trend the effect of stochastic sampling must be relatively small.

We investigate this point more closely in Figure 2. This figure shows stellar isochrones for both optical and NIR filters for 8 SSPs produced by the PARSEC v1.1 models of Bressan et al. (2012, 2013). The colored circles at the top of the plot show the total integrated color of the SSPs for a Chabrier lognormal IMF. From this plot it is clear that the colors of the main sequence turnoff (which dominates the overall color) and the extreme RGB differ by at most 0.1 mag in the NIR, but by up to 1.1 mag in the optical, hence population of the extreme RGB does little to change the color of the population for NIR bands.

2.2. Stellar Population Samples

2.2.1. Milky Way and Magellanic Cloud Globular Clusters

We selected an initial sample of MW GCs drawn from the Harris 1996 (2010 edition) catalog, supplemented with a sample of Large and Small Magellanic Cloud GCs drawn from McLaughlin & van der Marel (2005). The

² <http://wise2.ipac.caltech.edu/docs/release/allwise>

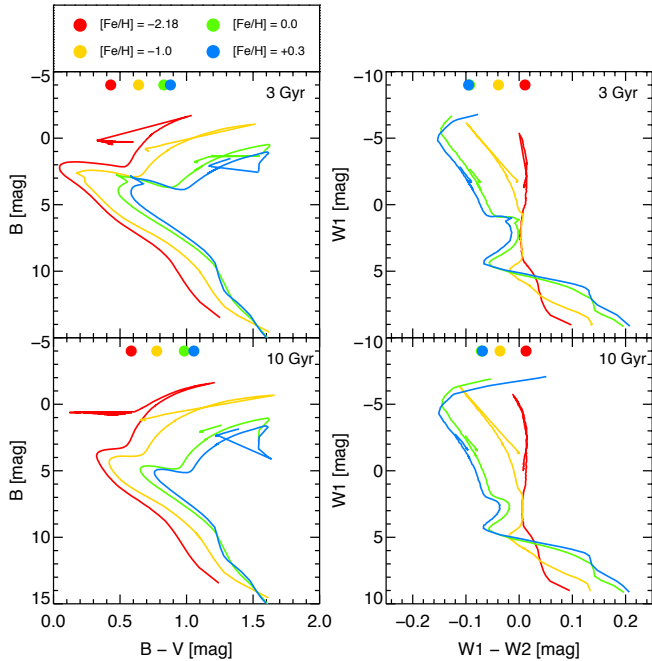


Figure 2. Stellar isochrones for single stellar populations from the Bressan et al. (2012, 2013) models for both B - V (left panels) and W1 - W2 (right panels). The upper panels show the isochrones for 3 Gyr stellar populations, and the lower panels are 10 Gyr SSPs. The colors represent different metallicities as indicated in the legend at the top. The colored circles at the top in each panel show the total integrated color of each SSP assuming a Chabrier IMF and a fully populated isochrone. The integrated color is dominated by the color of stars on or near the main sequence turnoff, but only in the optical case do red giant branch stars have colors that differ considerably from this average color. Note also that the metallicity dependence of the color is reversed for the NIR colors with more metal rich isochrones becoming bluer in the NIR case.

sample was created by requiring the GCs to 1) have a measured age and metallicity, 2) to be older than 2 Gyr, 3) be more luminous than $M_V = -7.00$, and 4) yet not saturated in the WISE imaging, and finally 5) to have half-light radii ($R_e > 10''$) that are well resolved by the W1 and W2 photometry. The third requirement ensures that the GCs are sufficiently massive that the effect of stochastic variation in the population of their red giant and horizontal branches is negligible (see Section 2.1). The fourth requirement is more subtle, as the ALLWISE combination algorithm tends to hide saturation in the final images in all but the most extreme cases. As saturation is more common in the W1 band this can lead to spurious color trends. Only by checking the single epoch WISE exposures manually was it possible to be certain that the atlas images were unaffected by saturation.

By applying these requirements (and a subsequent cut on the photometric uncertainty of the W1 - W2 color) we are left with a final sample of 66 MW and Magellanic Cloud GCs. Unfortunately because of the saturation problems, which preferentially effect closer and higher metallicity MW GCs, the sample has relatively few GCs with metallicity $[\text{Fe}/\text{H}] > -1$.

Each cluster was analysed in the following manner:

1. The ALLWISE Atlas science and uncertainty images for each cluster were downloaded.
2. Using the literature values of GC center, position

angle, ellipticity (generally negligible for GCs) and R_e , an aperture containing half the GC light was defined and the flux summed within this region. The value of R_e was determined from optical data and was therefore scaled by a factor of 0.71 to account for the fact that the half-light radius is smaller in IR bands (Falcón-Barroso et al. 2011). Summing the flux within R_e ensures that the flux of the GC dominates and the influence of background sources is negligible. It also ensures that we can measure the flux within a single aperture, rather than have to carry out the uncertain task of identifying and measuring individual cluster stars at large radii where the field contamination becomes significant.

3. SExtractor (Bertin & Arnouts 1996) was used to determine a background map, after masking the GC, and using a very large BACK_SIZE value of 512 pixels to ensure that the influence of foreground and background sources was reduced.
4. The “sky” background was then subtracted from the total GC flux in each band, the magnitudes and their uncertainties calculated and the standard conversions to the WISE magnitude system applied (Wright et al. 2010).

2.2.2. M31 Globular Clusters

To augment the MW GC sample we also make use of WISE photometry of spectroscopically confirmed M31 GCs drawn from the Revised Bologna Catalog of M31 GCs (RBC; Galleti et al. 2004). To the RBC we add additional age and metallicity measurements from the literature (Ma et al. 2009; Wang et al. 2010; Caldwell et al. 2011; Cezario et al. 2013) to produce the largest possible catalog of spectroscopically confirmed M31 GCs with stellar population measurements.

We apply similar requirements to those used for the MW GC system. We also require spectroscopic confirmation of their nature, as the RBC catalog suffers from significant contamination from foreground and background objects (see e.g. Huxor et al. 2014). Saturation of the WISE imaging is not an issue for M31 GCs due to the increased distance relative to the MW GCs, however, we do visually inspect each cluster to reject those cases where the photometry is likely compromised by bright nearby sources.

After this selection we are left with a sample of 61 M31 GCs, with metallicities that range from $[\text{Fe}/\text{H}]$ of -1.9 to -0.1 . The photometry for the M31 GC sample is taken directly from the catalog measurements for the ALLWISE data release. In this case we do apply an extinction correction, as some of the GCs are observed in (and even behind) the disk of M31. Where available we make use of the Caldwell et al. (2011) estimations of $E(B-V)$, because these include the foreground MW extinction and the effects of the internal M31 extinction. Where our GCs lack $E(B-V)$ measurements we use the median value of the $E(B-V)$ for the M31 GCs as determined by Caldwell et al. (2011). We then convert the $E(B-V)$ into extinctions in the W1 and W2 bands using the conversions quoted in Yuan et al. (2013).

2.2.3. Early-Type Galaxies

In addition to the GC samples we also examine the WISE colors of early-type galaxies (ETGs). Our main ETG sample is that of the SAURON survey (de Zeeuw et al. 2002). This contains of 48 nearby S0 and E galaxies observed with the SAURON spectrograph on the WHT telescope (Bacon et al. 2001). The NIR colors of these galaxies have already been examined by Peletier et al. (2012), who used Spitzer IRAC imaging of the sample galaxies to measure their $[3.6] - [4.5]$ colors, finding that galaxies became increasingly blue with increasing metallicity, in marked contrast to the behavior for most other colors. The principle limitation of the SAURON sample is that the metallicity range is quite restricted, with most galaxies having $-0.5 < [\text{Fe}/\text{H}] < 0$. Therefore we have extended the metallicity range probed by the galaxy sample by adding additional dwarf and giant early type galaxies to the sample.

In order to be considered for inclusion in our extended galaxy sample several properties had to be available in the literature. These comprised suitable photometric values for effective radius, position angle, and ellipticity as well as spectroscopically determined age and metallicity, (ideally weighted to be within R_e). Such information was compiled from the literature sources listed below, occasionally supplemented by position angles and ellipticities provided by either Hyperleda (Paturel et al. 2003) or the SDSS data release 10 (Ahn et al. 2014).

We added several lower mass dE and dS0 galaxies from the work of Ryś et al. (2013, 2014). These galaxies were observed using the SAURON spectrograph similar to the main SAURON sample, with their stellar populations (Rys et al. in prep) also derived in a manner consistent with the rest of the SAURON sample.

We also added additional dwarf and giant early-type galaxies using derived properties provided in the papers of Michielsen et al. (2008); Koleva et al. (2011); Forbes et al. (2011).

Finally, we added higher-mass early-type galaxies from the study of Denicoló et al. (2005). In this case we converted their measured central metallicity to an approximate half-light weighted metallicity by subtracting the mean offset between the R_e and $R_e/8$ derived metallicities of the SAURON sample.

Where necessary (for example with the SAURON sample) we convert their measured $[\text{Z}/\text{H}]$ metallicity estimates to $[\text{Fe}/\text{H}]$ using the relation that $[\text{Z}/\text{H}] = [\text{Fe}/\text{H}] + 0.94 \times [\alpha/\text{Fe}]$ (Thomas et al. 2003).

We analyse the full galaxy sample in the same way as the MW GCs, i.e. we measure the WISE photometry within ellipses set by the observed ellipticity, position angle and R_e of the galaxies. Figure 3 displays an example of this procedure. Likewise we restrict the sample selected for study using the same limitations, for example we only study those objects which have $R_e > 10''$ to ensure that the half-light radius is adequately resolved in the WISE imaging. We also limit our analysis to galaxies which have age > 2 Gyr, to ensure that the effect of poorly understood evolved stellar phases such as thermally pulsating asymptotic giant branch (TP-AGB) is significantly reduced (see e.g. Maraston 2005).

3. RESULTS

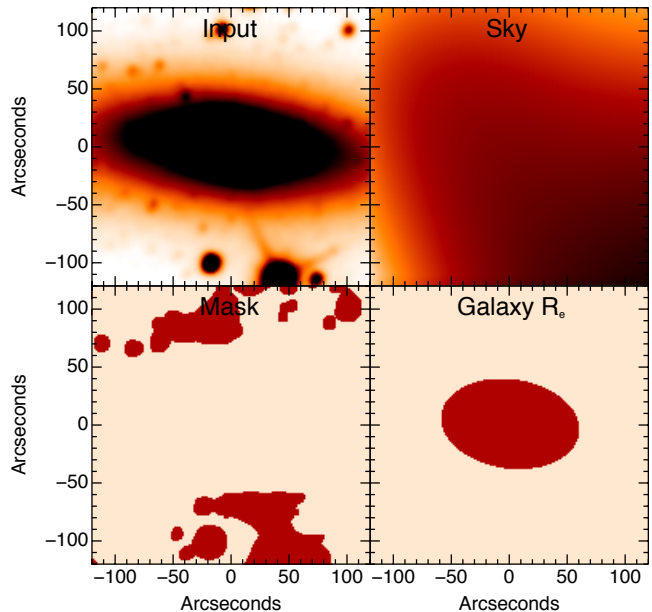


Figure 3. Photometric analysis of the early-type galaxy NGC 1023. **Top Left** : Zoomed region of the input WISE W1 image. **Top Right** : The SExtractor derived sky map (with stretch altered to enhance spatial variability). No obvious sign of influence from the galaxy itself can be seen. **Bottom Left** : The SExtractor derived masked regions. **Bottom Right** : The elliptical half-light isophote.

3.1. W1-W2 colors of Old Stellar Populations

The left panel of Figure 4 displays the W1 - W2 colors of our sample of old stellar systems plotted against their metallicity. The solid and dashed black and white lines are the running average of the whole sample and the 1σ scatter, as measured in 0.25 dex bins. It is clear from this plot that there is a highly significant trend, with the stellar populations becoming bluer with increasing metallicity, as was found previously by Peletier et al. (2012); Meidt et al. (2014) for the IRAC $[3.6] - [4.5]$ μm color. The running average of the points is well reproduced by a linear relation between metallicity and W1-W2 color of the following form:

$$W1 - W2 = -0.026 \times [\text{Fe}/\text{H}](\text{dex}) - 0.058 \quad (1)$$

with the scatter about the relation being 0.026 magnitudes.

The right panel of Figure 4 displays the same data, but overlaid with several current SPS model predictions. The SPS models fall into two groups; those that attempt to correct for the CO absorption in the W2 band (the PARSEC v1.1 models of Bressan et al. 2012, 2013, the earlier Padova group models of Marigo et al. 2008 using the Girardi et al. 2010 TP-AGB tracks, and the Meidt et al. 2014 corrected Bruzual & Charlot 2003 models), and those that do not (the Bruzual & Charlot 2003, the GALEV models of Kotulla et al. 2009, and the FSPS model of Conroy et al. 2009b; Conroy & Gunn 2010).

It is clear that the majority of the models, including those most commonly used to derive stellar population properties and stellar masses dramatically fail to reproduce the W1 - W2 colors of stellar populations with near solar metallicity. Only those models that include

the effect of the increasing CO absorption strength at $4.5\mu\text{m}$ successfully reproduce the observed trend. Both the Padova group models and the empirical model fit the data reasonably, with the empirical model of Meidt et al. (2014) being slightly more consistent with the data overall.

Note that, based on the behavior of the Bressan et al. (2012, 2013) models, the W1 - W2 color is almost insensitive to age for stellar populations > 2 Gyr. We therefore do not expect that age contributes significantly to the observed scatter here, which is large even for relatively bright stellar systems. Such large observational scatter unfortunately prevents us currently using W1-W2 color as an accurate metallicity indicator. Still, we note that improvements in data quality may allow the use of the W1-W2 color may act as a useful a prior on metallicity, e.g. to help break the well-known age-metallicity relation in the optical.

3.2. The Absolute Zeropoint in the W1 & W2 Bands

In order to confirm the zero point of the models in the WISE filter system we can use the models to predict the absolute magnitude of the Sun in the WISE bands.

The Bressan et al. (2012, 2013) PARSEC v1.1 isochrones give the absolute magnitude of a solar mass star with a solar abundance and age 4.6 Gyr as $W1 = 3.24$ and $W2 = 3.26$. These values are remarkably close to the values of 3.24 and 3.27 as determined by Jarrett et al. (2013) for W1 and W2 based on the WISE relative system response and the SED of the Sun. The Marigo et al. (2008) models likewise predict solar magnitudes very close to the observed values; 3.22 and 3.24 magnitudes, respectively.

In contrast, while the remaining models (BC03, FSPS, and GALEV) do approximately give the correct value for the magnitude of the sun in the W1 band, as expected from their predictions of the W1 - W2 color (see Section 3.1), they substantially underpredict the absolute magnitude of the Sun in the W2 band.

As the PARSEC models correctly predict both the absolute zero point, and the color behavior of the W1 and W2 filters we therefore choose to examine further whether these models and bands can be used to produce a widely applicable stellar mass estimator.

3.3. Mass-to-light ratios at 3.4 and $4.6\mu\text{m}$

Having demonstrated that some modern SPS models are capable of reproducing the observed WISE W1 and W2 photometry of dust-free stellar populations we now examine what these models predict for the mass-to-light ratio behavior of simple stellar populations.

To do this we make use of the PARSEC v1.1 models (Bressan et al. 2012, 2013) for a Chabrier lognormal IMF and single burst models (i.e. pure SSPs) which we convert to mass-to-light ratios assuming that the mass remaining in living stars and remnants follows the tracks presented in Into & Portinari (2013) for a Kroupa IMF (i.e. $\sim 30\%$ of the stellar mass is returned to the ISM within 12 Gyr). Figure 5 shows the result of this procedure for a range of 4 metallicities (from $[\text{Fe}/\text{H}] = -2.18$ to $+0.3$) and eight ages from 0.5 Gyr to 10 Gyr. It is important to note that because the current v1.1 of the PARSEC models do not include the effects of TP-AGB

stars, the predictions for ages < 3 Gyr are likely to be significantly in error. However, comparison with the Marigo et al. (2008) models, which are an earlier iteration of the Padova models which do include the effects of TP-AGB, shows that for ages > 3 Gyr the predicted M_*/L ratios seem to be robust.

Examining Figure 5 it is immediately obvious that in common with the conclusions of Meidt et al. (2014) we find that for metallicities displayed by modern galaxies (i.e. $[\text{Fe}/\text{H}] > -1$) the M_*/L ratios are essentially insensitive to metallicity (and hence color). It is also notable that in the age range of 3 to 10 Gyr, the M_*/L ratio increases by around a factor of two, meaning that applying a fixed M_*/L ratio in the middle of the range leads to errors on the derived stellar mass of only 0.10 dex. This is also in good agreement with the analysis of Meidt et al. (2014), who using their modified Bruzual & Charlot (2003) models found that for exponentially declining star formation histories (which tend to reduce the overall M_*/L when compared to single burst histories) it was possible to use a single M_*/L of 0.6 to derive stellar masses from IRAC [3.6] photometry with 0.10 dex uncertainties.

As expected, the derived M_*/L ratios for the 3.4 and $4.6\mu\text{m}$ bands are very similar, and that therefore both have the potential to be useful stellar mass indicators. In general the $3.4\mu\text{m}$ band is likely to be preferred due to the higher S/N of the WISE imaging in this band. However, in certain cases, the $4.6\mu\text{m}$ flux may be a more robust tracer of old stellar light, e.g. when the $3.4\mu\text{m}$ bandpass also contains strong $3.3\mu\text{m}$ PAH emission. This effect is likely negligible for the old stellar populations in this study.

3.4. Stellar Masses

In order to check the efficacy of the M_*/L ratios in Section 3.3 we compare WISE derived stellar masses to those determined by the ATLAS3D survey (specifically the Salpeter masses from Cappellari et al. 2013) for the 47 galaxies in common with the SAURON survey. We study only the SAURON survey galaxies instead of the full ATLAS3D sample because spectroscopically determined stellar population parameters (from Kuntschner et al. 2010) are only available currently for the SAURON subset. This allows us to examine the improvement in derived stellar masses when the additional information provided by the age and metallicity of the galaxies are included. We choose to use the ATLAS3D Salpeter stellar masses because these masses are computed using the input provided by a spectroscopically-derived smoothed star formation history. This procedure should therefore reduce the confusing effect of SFH on derived stellar masses, and provide a more robust stellar mass for comparison to our WISE derived stellar masses.

To determine the WISE stellar masses our approach is very simple. We take the W1 and W2 luminosity of the galaxies measured within R_e as described in Section 2.2.3 and double it to account for the flux outside the half-light aperture. To ensure consistency with the ATLAS3D studies we use their distance measurements for each galaxy. Once we have the total luminosity of each galaxy we then use two different approaches to derive the final stellar mass. The simplest approach is to apply a fixed M_*/L , this is chosen arbitrarily to match the zero

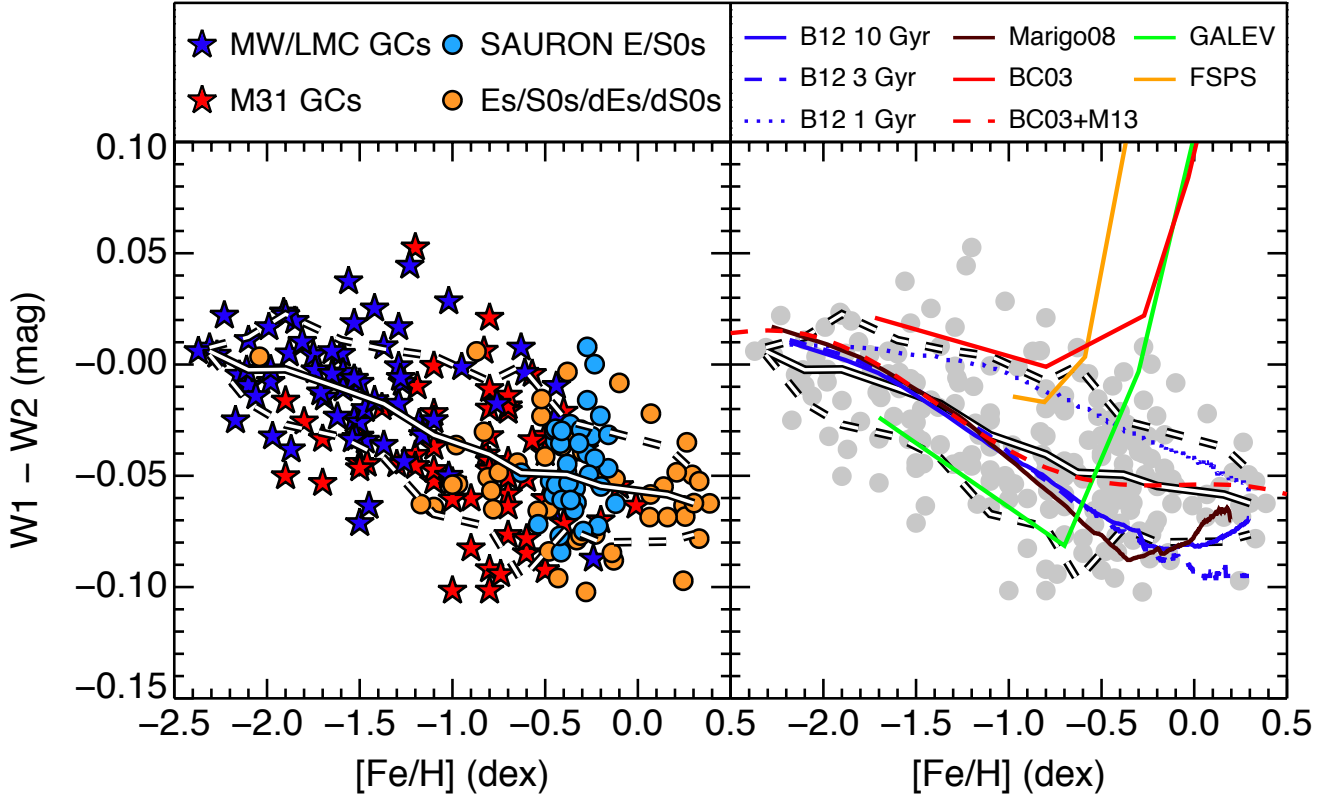


Figure 4. Left Panel : The $W1 - W2$ colors of our sample of dust-free stellar systems plotted against their metallicity. The blue stars are MW and Magellanic Cloud GCs, the red stars are M31 GCs, the cyan circles are the SAURON sample galaxies, and the orange circles are the remaining dwarf and giant early-type galaxies (See Section for details). The black-and-white solid line shows the running average of the whole sample, as determined in 0.25 dex bins, the black-and-white dashed lines are the 1σ scatter on the running average. **Right Panel :** The grey circles show the entire sample, now undifferentiated by stellar system type or source. The solid and dashed black-and-white lines show the same running mean and 1σ scatter from the left panel. The blue lines show predictions of the Bressan et al. (2012, 2013) SPS model for stellar populations with ages of 1 Gyr (dotted line), 3 Gyr (dashed line), and 10 Gyr (solid line). All remaining models are for 10Gyr SSPs: The brown solid line shows the Marigo et al. (2008) model with the Girardi et al. (2010) TP-AGB tracks. The solid red line shows the Bruzual & Charlot (2003) prediction, while the dashed red line shows Bruzual & Charlot (2003) prediction after empirical correction for the effects of the $4.5\mu\text{m}$ CO feature by Meidt et al. (2014). The solid green line shows the prediction from the GALEV model of Kotulla et al. (2009). Finally the solid orange line shows the prediction from the FSPS models of Conroy et al. (2009b) and Conroy & Gunn (2010).

point of the ATLAS3D masses (once they have been offset by the standard $+0.25$ dex to account for differences between a Chabrier and Salpeter IMF). The second approach is to use the measured stellar population parameters of each galaxy to determine the appropriate M_*/L through interpolation of the relations shown in Figure 5.

Figure 6 displays the results of these procedures for both the $W1$ (upper panels) and $W2$ (lower panels) bands. From the left panels of the figure, which display the result of using fixed M_*/L ratios, it is obvious that the relation is remarkably tight, with most of the significant outliers being known young galaxies (the blue dots without black border) where the chosen M_*/L is particularly inappropriate. It should be noted that the derived values of M_*/L (0.85 and 0.88 in $W1$ and $W2$ respectively) are likely consistent with 0.6 value derived by Meidt et al. (2014) when it is considered that our M_*/L ratio likely includes some systematic offset caused by missing galaxy light due to our method of doubling the flux within half-light apertures, especially as the half-light radii are determined in optical bands not directly from the WISE imaging. In fact, if matched apertures are used (i.e. the WISE apertures are matched to the ones used by the SAURON survey) the M/L ratios become 0.67 and 0.70 for the $W1$ and $W2$ bands respectively,

even more consistent with the 0.6 value derived by Meidt et al. (2014). The observed scatter in the $3.4\mu\text{m}$ relation is also remarkably close to the value of 0.1 dex predicted by Meidt et al. (2014), all the more remarkable when it is considered that the errors in the ATLAS3D stellar mass determinations must also be considerable.

The right panels display the effect of using M_*/L s determined using the stellar population parameters, in this case no offsetting to match the ATLAS3D determinations is done. Several interesting effects are apparent in these panels:

1. The offsets of the younger galaxies from the one-to-one line are significantly reduced, due to their now having more appropriate (and lower) M_*/L than in the fixed M_*/L case.
2. Secondly, there is a significant offset between the ATLAS3D and WISE mass determinations, (i.e. the average ratio $M_{\text{ATLAS3D}}/M_{3.4\mu\text{m}}$ is 0.86 not 1.) in the sense that the WISE determinations are higher. The fact that the magnitude of this offset is very similar for both $W1$ and $W2$ indicates that this could be related to the method used to determine the total luminosity in the WISE bands,

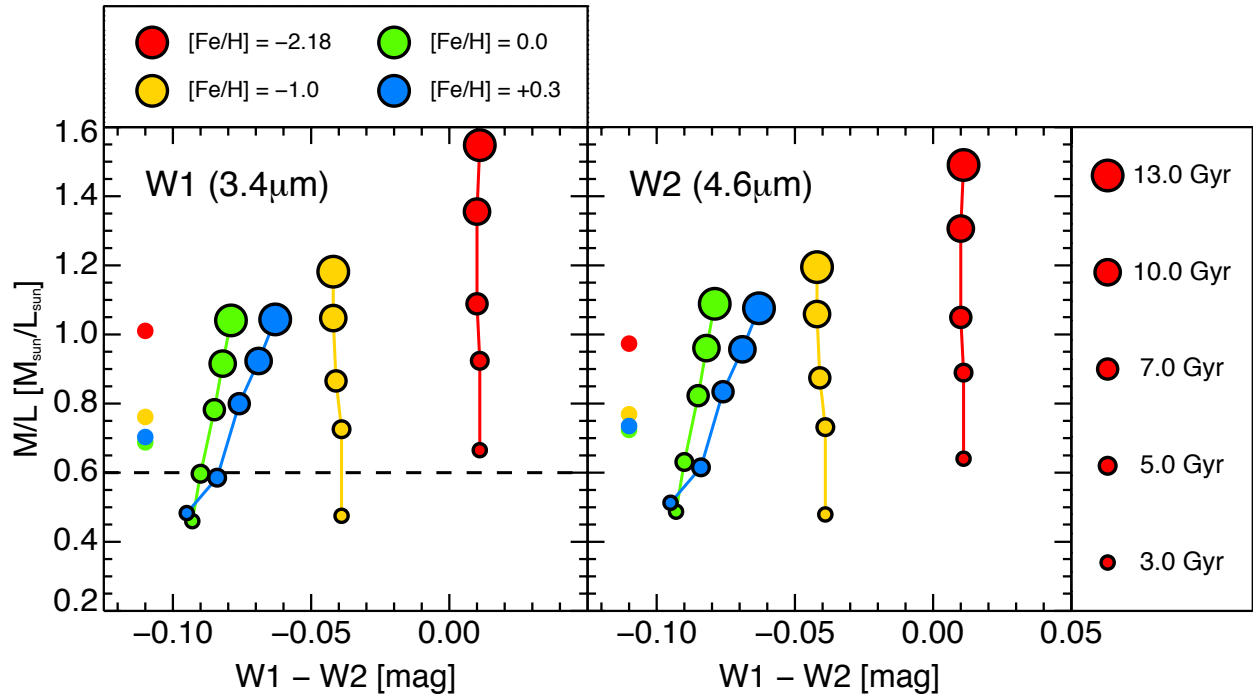


Figure 5. The W1 - W2 color vs 3.4 and 4.6 μm mass-to-light ratios derived from the PARSEC v1.1 models of Bressan et al. (2012, 2013) as described in Section 3.3. Single stellar populations for combinations of four metallicities ranging from -2.18 to $+0.3$, and ages from 3 to 13 Gyr are displayed. The colored dots to the left of each panel without black outline display the average M_*/L for SSPs with age between 3 and 10 Gyr ($M_*/L_{W1} = 1.01, 0.76, 0.69$ and 0.70 for the 4 metallicities plotted). The dashed line in the left panel displays the M_*/L of 0.6 suggested by Meidt et al. (2014) as a suitable fixed M_*/L for old stellar populations, based on Bruzual & Charlot (2003) models with exponentially declining star formation histories. As noted by Meidt et al. (2014) the mass-to-light ratio increases by a factor of around 2 between 3 and 10 Gyr.

and that we have systematically overestimated the total luminosity, or, alternatively, that the stellar population parameters (principally the ages) determined by the SAURON survey are differ systematically from those used by the ATLAS3D survey in their analysis.

3. A third observation is that the scatter is reduced compared to that found for the fixed M_*/L case. When it is considered that the ATLAS3D stellar masses contribute a significant fraction of the total scatter the magnitude of the decrease is even more remarkable.
4. Finally, and most intriguingly, there is evidence that the relation is no longer one-to-one, in the sense that the WISE derived masses are increasingly over-massive compared to the ATLAS3D ones for higher mass galaxies. We leave a more detailed investigation of this point to a forthcoming paper.

4. DISCUSSION

We have used NIR WISE photometry of a diverse sample of old stellar systems to probe the behavior of these stellar systems as a function of the full metallicity range displayed by star clusters and galaxies. Using this sample we have confirmed that the latest generation of stellar population synthesis models (in particular the Padova group models of Bressan et al. 2012, 2013) are capable of accurately reproducing the colors and luminosities of the 3.4 and 4.6 μm bands for old stellar systems.

Having confirmed that the SPS models accurately reproduce the NIR photometry of real stellar systems, we then made use of the models to derive mass-to-light ratios for single burst stellar populations as a function of metallicity and age. As found by Meidt et al. (2014) for the IRAC 3.6 μm band this procedure demonstrated that the WISE W1 and W2 M_*/L ratios are almost insensitive to metallicity for $[\text{Fe}/\text{H}] > -1$ dex. Furthermore, by comparison with the stellar masses derived by the ATLAS3D survey we confirmed that the use of a single fixed M_*/L in the NIR for galaxies older than 3 Gyr can produce remarkably accurate stellar mass estimates.

Having confirmed that modern SPS models can be used to accurately predict stellar masses for older stellar populations several further steps can be envisaged to make the technique more widely applicable. In order to extend this technique to younger stellar populations several confusing effects will have to be integrated into the models or the analysis procedure. The most pressing is to include the effect of evolved stellar phases such as TP-AGB stars, which can contribute significantly to the total luminosity in the NIR for ages < 3 Gyr, even in cases where the galaxy (though not the AGB stars) itself may be relatively dust-free. Implementation of this change is already underway by the Padova group and other SPS modellers.

A second necessary step will be to determine and remove the effect of non-stellar emission in the NIR bands, particularly in the 3.6 μm band, where a PAH emission feature is present. Removal of non-stellar emission could potentially be achieved using several approaches, one would be to use independent component analysis such

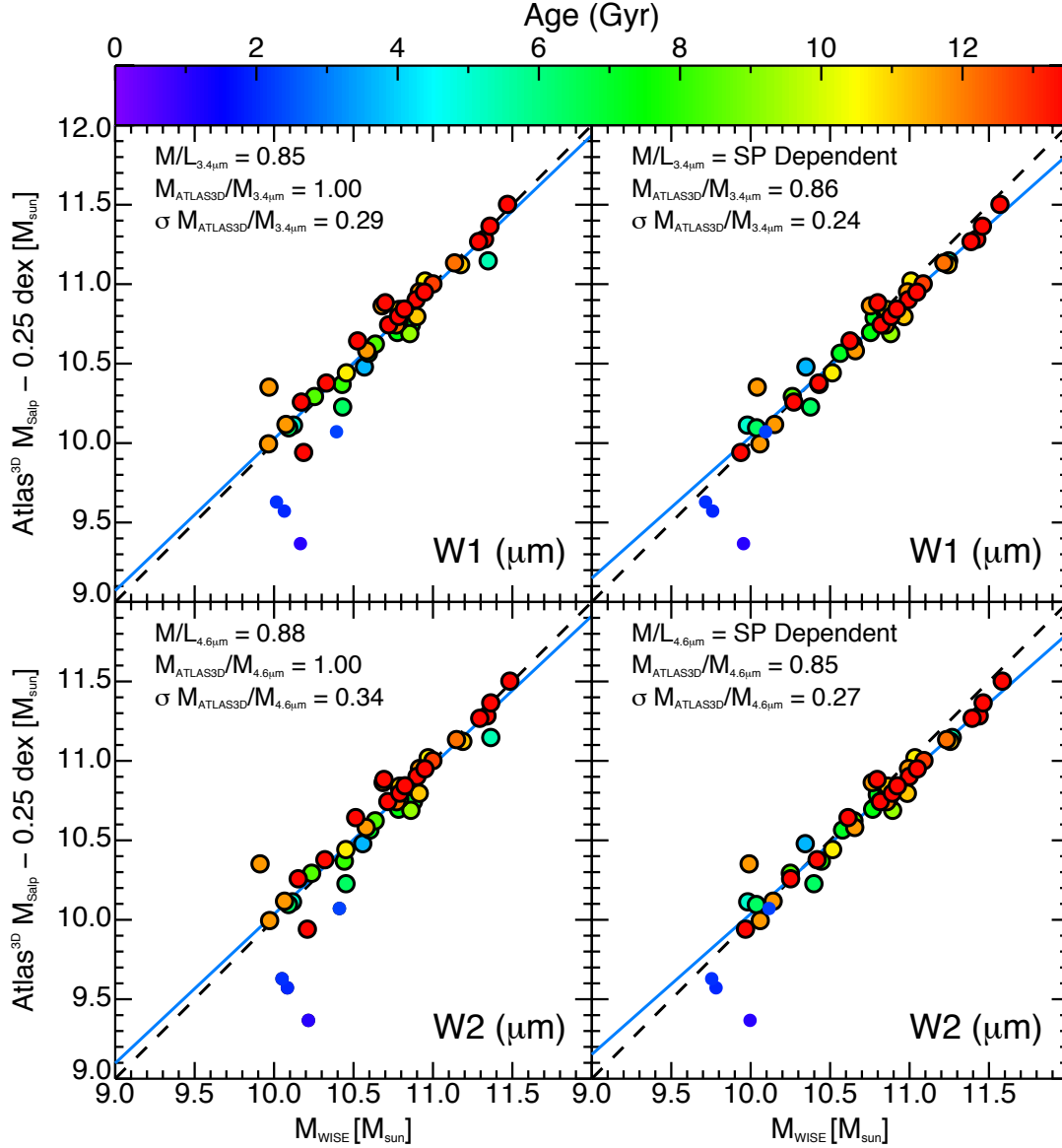


Figure 6. The WISE W1 and W2 derived stellar masses for the SAURON survey (de Zeeuw et al. 2002) galaxies vs the stellar masses derived for the same galaxies by the ATLAS3D survey (Cappellari et al. 2011). In each panel the color of the dots gives the luminosity weighted SSP age as measured by Kuntschner et al. (2010). Those galaxies which have measured age within R_e of > 3 Gyr have a black outline, those younger than 3 Gyr do not. The dashed line in each panel shows the one-to-one relation, while the solid blue line is the best fit linear relation for those galaxies with age > 3 Gyr. The stellar masses from the ATLAS3D survey are the Salpeter IMF masses from Cappellari et al. (2013) scaled by 0.25 dex to account for the difference between the Salpeter IMF and the Chabrier IMF assumed for the WISE measurements. The upper panels show the results for the W1 ($3.4\mu\text{m}$) band and the lower panels for the W2 ($4.6\mu\text{m}$) band. The left panels show the result when the W1 and W2 mass-to-light ratios are fixed for all galaxies, at a value chosen arbitrarily to match the ATLAS3D masses, but consistent with a stellar population with age ~ 9 Gyr (see Figure 5). The right panels show the effect of varying the mass-to-light ratio based on the SAURON measured stellar populations (presented in Kuntschner et al. 2010). The top right of each panel shows the band used, the method used to determine M_*/L , and both the ratio between ATLAS3D mass and WISE mass and the scatter around this ratio for galaxies older than 3 Gyr.

as was used for the S⁴G sample by Meidt et al. (2012) and Querejeta et al. (2014). An alternative approach that could be more successful for poorly resolved (or entirely un-resolved) sources might be to make use of the W3 band as a probe of the non-stellar emission and to use this to correct the W1 photometry.

5. CONCLUSIONS

We have presented the first large sample size examination of the dust-free NIR photometry of older stellar populations as a function of the full metallicity range displayed by globular clusters and galaxies. Our main

conclusions are:

1. Contrary to the predictions of the majority of SSP models the W1-W2 colors of stellar populations become systematically *bluer* with increasing metallicity.
2. Using SPS models which fit the observed color-metallicity relations, and hence accurately predict both the 3.4 and $4.6\mu\text{m}$ fluxes we derive mass-to-light ratios for both the WISE W1 and W2 filters. In doing this we determined that for the range of

metallicities encountered in massive galaxies the M_*/L in the NIR is relatively insensitive to metallicity, and in the case of age, varies by a factor of 2 between 3 and 10 Gyr.

3. By comparison of our WISE-derived stellar masses with a SAURON+ATLAS3D sample of early-type galaxies we confirm the finding of Meidt et al. (2014) that a single fixed M_*/L at $3.4\mu\text{m}$ can produce stellar masses with uncertainties of only 0.1 dex.
4. We find that when including additional age information the accuracy of the derived stellar masses can be improved by a further 0.02 dex for dust free stellar populations older than 3 Gyr.

6. ACKNOWLEDGEMENTS

We would like to thank Benjamin Röck for useful discussions regarding modelling the NIR emissions of old stellar populations.

We would like to thank Agnieszka Rys for providing the measured stellar population parameters for her sample of dwarf galaxies ahead of publication.

This publication makes use of data products from the Wide-field Infrared Survey Explorer, which is a joint project of the University of California, Los Angeles, and the Jet Propulsion Laboratory/California Institute of Technology, and NEOWISE, which is a project of the Jet Propulsion Laboratory/California Institute of Technology. WISE and NEOWISE are funded by the National Aeronautics and Space Administration.

We acknowledge financial support to the DAGAL network from the People Programme (Marie Curie Actions) of the European Unions Seventh Framework Programme FP7/2007- 2013/ under REA grant agreement number PITN-GA-2011-289313

We acknowledge the usage of the HyperLeda database (<http://leda.univ-lyon1.fr>).

This research has made use of the NASA/IPAC Extragalactic Database (NED) which is operated by the Jet Propulsion Laboratory, California Institute of Technology, under contract with the National Aeronautics and Space Administration.

Funding for SDSS-III has been provided by the Alfred P. Sloan Foundation, the Participating Institutions, the National Science Foundation, and the U.S. Department of Energy Office of Science. The SDSS-III web site is <http://www.sdss3.org/>.

SDSS-III is managed by the Astrophysical Research Consortium for the Participating Institutions of the SDSS-III Collaboration including the University of Arizona, the Brazilian Participation Group, Brookhaven National Laboratory, Carnegie Mellon University, University of Florida, the French Participation Group, the German Participation Group, Harvard University, the Instituto de Astrofísica de Canarias, the Michigan State/Notre Dame/JINA Participation Group, Johns Hopkins University, Lawrence Berkeley National Laboratory, Max Planck Institute for Astrophysics, Max Planck Institute for Extraterrestrial Physics, New Mexico State University, New York University, Ohio State University, Pennsylvania State University, University of Portsmouth, Princeton University, the Spanish Participation Group,

Name	[Fe/H] [dex]	W1 - W2 [mag]
Milky Way Globular Clusters		
NGC 1261	-1.27	-0.008 ± 0.009
Pal2	-1.42	0.025 ± 0.012
NGC 1851	-1.18	-0.026 ± 0.009
NGC 1904	-1.60	0.005 ± 0.009
NGC 2419	-2.15	-0.005 ± 0.019
NGC 3201	-1.59	-0.011 ± 0.012
NGC 4590	-2.23	0.022 ± 0.010
NGC 4833	-1.85	0.020 ± 0.012
NGC 5024	-2.10	-0.009 ± 0.010
ω Cen	-1.53	0.019 ± 0.010
NGC 5272	-1.50	-0.008 ± 0.009
NGC 5286	-1.69	-0.015 ± 0.009
NGC 5634	-1.88	0.005 ± 0.009
NGC 5694	-1.98	-0.008 ± 0.036
IC4499	-1.53	-0.025 ± 0.026
NGC 5824	-1.91	0.023 ± 0.009
NGC 5897	-1.90	0.022 ± 0.015
NGC 5904	-1.29	-0.018 ± 0.019
NGC 5946	-1.29	-0.001 ± 0.015
NGC 5986	-1.59	-0.004 ± 0.009
NGC 6093	-1.75	0.004 ± 0.009
NGC 6139	-1.65	0.006 ± 0.010
NGC 6171	-1.02	0.028 ± 0.010
NGC 6205	-1.53	-0.006 ± 0.009
NGC 6229	-1.47	-0.034 ± 0.009
NGC 6218	-1.37	0.008 ± 0.009
NGC 6254	-1.56	0.037 ± 0.009
NGC 6273	-1.74	-0.003 ± 0.011
NGC 6284	-1.26	-0.044 ± 0.011
NGC 6287	-2.10	0.011 ± 0.011
NGC 6293	-1.99	0.017 ± 0.019
NGC 6316	-0.45	-0.025 ± 0.021
NGC 6341	-2.31	0.008 ± 0.009
NGC 6402	-1.28	-0.006 ± 0.009
NGC 6496	-0.46	-0.065 ± 0.018
NGC 6517	-1.23	0.044 ± 0.012
NGC 6539	-0.63	0.008 ± 0.014
NGC 6541	-1.81	0.010 ± 0.009
NGC 6569	-0.76	-0.018 ± 0.020
NGC 6584	-1.50	-0.026 ± 0.011
NGC 6624	-0.44	-0.010 ± 0.012
NGC 6638	-0.95	-0.001 ± 0.013
NGC 6681	-1.62	-0.023 ± 0.010
NGC 6712	-1.02	-0.050 ± 0.028
NGC 6723	-1.10	-0.025 ± 0.017
NGC 6779	-1.98	-0.002 ± 0.010
NGC 6864	-1.29	0.017 ± 0.009
NGC 6934	-1.47	-0.020 ± 0.009
NGC 6981	-1.42	-0.016 ± 0.011
NGC 7006	-1.52	-0.033 ± 0.010
NGC 7078	-2.37	0.006 ± 0.009
NGC 7089	-1.65	-0.004 ± 0.009
NGC 7099	-2.27	0.004 ± 0.009

Table 1
Cataloged metallicity and WISE W1-W2 color as measured using the approach described in Section 2.2 and plotted in Figure 4.

University of Tokyo, University of Utah, Vanderbilt University, University of Virginia, University of Washington, and Yale University.

7. APPENDIX

Name	[Fe/H] [dex]	W1 - W2 [mag]
LMC and SMC Globular Clusters		
HODGE11	-2.06	-0.014 ± 0.020
NGC 1466	-2.17	-0.025 ± 0.016
NGC 1754	-1.54	-0.034 ± 0.022
NGC 1786	-1.87	-0.038 ± 0.008
NGC 1841	-2.11	-0.002 ± 0.030
NGC 1898	-1.37	-0.036 ± 0.015
NGC 2121	-0.61	-0.004 ± 0.032
NGC 2173	-0.24	-0.087 ± 0.014
NGC 2210	-1.97	-0.032 ± 0.012
KRON3	-1.16	-0.032 ± 0.035
NGC 121	-1.71	-0.013 ± 0.012
NGC 339	-1.50	-0.071 ± 0.043
NGC 361	-1.45	-0.064 ± 0.024
M31 Globular Clusters		
M31-B001	-0.70	-0.021 ± 0.043
M31-B004	-0.70	-0.077 ± 0.046
M31-B005	-0.70	-0.058 ± 0.037
M31-B006	-0.50	-0.060 ± 0.033
M31-B008	-0.80	-0.092 ± 0.045
M31-B012	-1.70	-0.033 ± 0.033
M31-B013	-0.50	-0.092 ± 0.050
M31-B017	-0.82	-0.040 ± 0.035
M31-B019	-0.80	-0.043 ± 0.033
M31-B020	-0.90	-0.060 ± 0.033
M31-B023	-0.70	-0.043 ± 0.030
M31-B024	-0.60	-0.085 ± 0.045
M31-B027	-1.30	-0.045 ± 0.048
M31-B034	-0.60	-0.078 ± 0.042
M31-B037	-0.80	-0.032 ± 0.035
M31-B039	-0.80	0.021 ± 0.040
M31-B045	-0.90	-0.083 ± 0.037
M31-B050	-0.80	-0.011 ± 0.050
M31-B051	-0.80	-0.102 ± 0.039
M31-B058	-1.10	-0.037 ± 0.035
M31-B061	-0.70	-0.019 ± 0.042
M31-B063	-0.80	-0.020 ± 0.034
M31-B068	-0.20	-0.070 ± 0.047
M31-B074	-1.50	-0.044 ± 0.049
M31-B082	-0.70	-0.064 ± 0.035
M31-B088	-1.80	-0.026 ± 0.034
M31-B094	-0.40	-0.071 ± 0.035
M31-B110	-0.70	-0.050 ± 0.042
M31-B116	-0.60	-0.051 ± 0.040
M31-B135	-1.46	-0.045 ± 0.047
M31-B158	-0.74	-0.094 ± 0.033
M31-B163	-0.29	-0.038 ± 0.043
M31-B174	-1.00	-0.061 ± 0.040
M31-B182	-1.00	-0.102 ± 0.037
M31-B183	-0.50	-0.040 ± 0.040
M31-B193	-0.10	-0.055 ± 0.041
M31-B212	-1.70	-0.053 ± 0.038
M31-B218	-0.80	-0.047 ± 0.038
M31-B219	-0.01	-0.063 ± 0.040
M31-B225	-0.44	-0.028 ± 0.033
M31-B232	-1.90	-0.016 ± 0.042
M31-B233	-1.10	-0.052 ± 0.044
M31-B238	-0.57	-0.004 ± 0.043
M31-B240	-1.50	-0.047 ± 0.035
M31-B301	-1.19	-0.010 ± 0.049
M31-B306	-1.10	-0.047 ± 0.033
M31-B311	-1.90	-0.050 ± 0.035
M31-B312	-1.20	-0.041 ± 0.035
M31-B313	-0.83	0.006 ± 0.039
M31-B344	-1.00	-0.053 ± 0.038
M31-B348	-1.38	-0.019 ± 0.044

Table 2
Table 1 cont.

Name	[Fe/H] [dex]	W1 - W2 [mag]
M31 Globular Clusters cont.		
M31-B352	-1.50	-0.032 ± 0.050
M31-B373	-0.50	-0.032 ± 0.040
M31-B379	-0.40	-0.021 ± 0.035
M31-B381	-1.10	-0.022 ± 0.037
M31-B383	-0.57	-0.034 ± 0.034
M31-B384	-0.70	-0.014 ± 0.035
M31-B386	-1.10	-0.001 ± 0.036
M31-B397	-1.20	0.053 ± 0.043
M31-B405	-1.20	-0.046 ± 0.033
SAURON Galaxies		
NGC 0474	-0.25	-0.032 ± 0.014
NGC 0524	-0.16	-0.032 ± 0.006
NGC 0821	-0.36	-0.027 ± 0.009
NGC 1023	-0.27	-0.040 ± 0.004
NGC 2549	-0.12	-0.063 ± 0.009
NGC 2685	-0.45	-0.034 ± 0.011
NGC 2695	-0.54	-0.072 ± 0.013
NGC 2768	-0.45	-0.030 ± 0.006
NGC 3377	-0.42	-0.036 ± 0.007
NGC 3379	-0.38	-0.048 ± 0.004
NGC 3384	-0.16	-0.047 ± 0.006
NGC 3414	-0.47	-0.052 ± 0.009
NGC 3489	-0.20	-0.023 ± 0.007
NGC 3608	-0.34	-0.056 ± 0.009
NGC 4150	-0.27	0.008 ± 0.014
NGC 4270	-0.33	-0.062 ± 0.018
NGC 4278	-0.46	-0.059 ± 0.006
NGC 4374	-0.44	-0.054 ± 0.004
NGC 4382	-0.31	-0.029 ± 0.004
NGC 4387	-0.41	-0.084 ± 0.017
NGC 4458	-0.63	-0.049 ± 0.019
NGC 4459	-0.32	-0.035 ± 0.006
NGC 4473	-0.34	-0.065 ± 0.006
NGC 4477	-0.37	-0.053 ± 0.007
NGC 4486	-0.44	-0.029 ± 0.003
NGC 4526	-0.27	-0.016 ± 0.005
NGC 4546	-0.42	-0.077 ± 0.007
NGC 4552	-0.21	-0.072 ± 0.005
NGC 4564	-0.29	-0.075 ± 0.010
NGC 4621	-0.41	-0.061 ± 0.005
NGC 5198	-0.36	-0.061 ± 0.014
NGC 5813	-0.41	-0.030 ± 0.008
NGC 5831	-0.23	-0.042 ± 0.011
NGC 5838	-0.26	-0.049 ± 0.008
NGC 5846	-0.38	-0.045 ± 0.006
NGC 5982	-0.20	-0.055 ± 0.009
NGC 7457	-0.23	0.000 ± 0.010

Table 3
Table 1 cont.

REFERENCES

- Ahn, C. P., Alexandroff, R., Allende Prieto, C., et al. 2014, ApJS, 211, 17
- Bacon, R., Copin, Y., Monnet, G., et al. 2001, MNRAS, 326, 23
- Barmby, P., Boyer, M. L., Woodward, C. E., et al. 2009, AJ, 137, 207
- Barmby, P., & Jalilian, F. F. 2012, AJ, 143, 87
- Bertin, E., & Arnouts, S. 1996, A&AS, 117, 393
- Bressan, A., Marigo, P., Girardi, L., Nanni, A., & Rubele, S. 2013, in European Physical Journal Web of Conferences, Vol. 43, European Physical Journal Web of Conferences, 3001
- Bressan, A., Marigo, P., Girardi, L., et al. 2012, MNRAS, 427, 127

Name	[Fe/H] [dex]	W1 - W2 [mag]
Other Dwarf and Giant ETGs		
VCC0308	-0.97	-0.054 ± 0.072
VCC0490	-0.35	-0.031 ± 0.081
VCC0523	-0.81	-0.051 ± 0.044
VCC0543	-0.41	-0.037 ± 0.076
VCC0634	-0.30	-0.039 ± 0.070
VCC0856	-0.43	-0.096 ± 0.085
VCC0929	-0.79	-0.057 ± 0.040
VCC1010	-0.33	-0.079 ± 0.041
VCC1036	-0.75	-0.048 ± 0.048
VCC1087	-1.10	-0.064 ± 0.060
VCC1261	-0.98	-0.036 ± 0.048
VCC1422	-0.48	-0.084 ± 0.057
VCC1861	-0.83	-0.030 ± 0.069
VCC1910	-0.13	-0.088 ± 0.053
VCC1912	-0.48	-0.065 ± 0.068
VCC2019	-0.28	-0.102 ± 0.098
NGC 3073	-0.87	0.006 ± 0.040
ID0650	-1.00	-0.054 ± 0.076
VCC0731	-0.14	-0.085 ± 0.006
VCC0828	-0.78	-0.065 ± 0.015
VCC1146	-1.17	-0.063 ± 0.022
VCC1279	-0.31	-0.077 ± 0.011
VCC1630	-0.54	-0.066 ± 0.017
VCC1903	-0.23	-0.076 ± 0.006
FCC021	0.07	-0.022 ± 0.003
FCC167	-0.21	-0.053 ± 0.008
FCC043	-0.50	-0.041 ± 0.045
FCC136	-0.65	-0.044 ± 0.084
FCC335	-0.52	-0.023 ± 0.054
NGC 205	-2.04	0.003 ± 0.005
NGC 404	-0.38	-0.003 ± 0.007
NGC 0720	0.25	-0.063 ± 0.006
NGC 1045	0.33	-0.078 ± 0.016
NGC 1132	-0.45	-0.055 ± 0.021
NGC 1407	0.29	-0.050 ± 0.006
NGC 1453	0.06	-0.069 ± 0.011
NGC 1700	0.14	-0.055 ± 0.010
NGC 2128	-0.10	-0.008 ± 0.013
NGC 2513	0.26	-0.068 ± 0.015
NGC 2911	0.26	-0.035 ± 0.014
NGC 3091	0.39	-0.062 ± 0.010
NGC 3226	-0.52	-0.016 ± 0.012
NGC 3607	0.30	-0.062 ± 0.006
NGC 3613	0.07	-0.058 ± 0.010
NGC 3640	0.21	-0.048 ± 0.008
NGC 3923	0.33	-0.052 ± 0.005
NGC 5812	0.24	-0.097 ± 0.012
NGC 5846A	-0.36	-0.053 ± 0.019
NGC 7302	0.16	-0.069 ± 0.017
NGC 7626	-0.12	-0.052 ± 0.011

Table 4
Table 1 cont.

Caldwell, N., Schiavon, R., Morrison, H., Rose, J. A., & Harding, P. 2011, *AJ*, 141, 61

Cappellari, M., Emsellem, E., Krajnović, D., et al. 2011, *MNRAS*, 413, 813

Cappellari, M., McDermid, R. M., Alatalo, K., et al. 2013, *MNRAS*, 432, 1862

Cezario, E., Coelho, P. R. T., Alves-Brito, A., Forbes, D. A., & Brodie, J. P. 2013, *A&A*, 549, A60

Conroy, C. 2013, *ARA&A*, 51, 393

Conroy, C., & Gunn, J. E. 2010, *ApJ*, 712, 833

Conroy, C., Gunn, J. E., & White, M. 2009a, *ApJ*, 699, 486

—. 2009b, *ApJ*, 699, 486

da Cunha, E., Charlot, S., & Elbaz, D. 2008, *MNRAS*, 388, 1595

de Zeeuw, P. T., Bureau, M., Emsellem, E., et al. 2002, *MNRAS*, 329, 513

Denicoló, G., Terlevich, R., Terlevich, E., Forbes, D. A., & Terlevich, A. 2005, *MNRAS*, 358, 813

di Serego Alighieri, S., Bianchi, S., Pappalardo, C., et al. 2013, *A&A*, 552, A8

Falcón-Barroso, J., van de Ven, G., Peletier, R. F., et al. 2011, *MNRAS*, 417, 1787

Forbes, D. A., Spitler, L. R., Graham, A. W., et al. 2011, *MNRAS*, 413, 2665

Fouesneau, M., & Lançon, A. 2010, *A&A*, 521, A22

Galleti, S., Federici, L., Bellazzini, M., Fusi Pecci, F., & Macrina, S. 2004, *A&A*, 416, 917

Girardi, L., Williams, B. F., Gilbert, K. M., et al. 2010, *ApJ*, 724, 1030

Harris, W. E. 1996, *AJ*, 112, 1487

Huxor, A. P., Mackey, A. D., Ferguson, A. M. N., et al. 2014, *ArXiv e-prints*, arXiv:1404.5807

Into, T., & Portinari, L. 2013, *MNRAS*, 430, 2715

Jarrett, T. H., Masci, F., Tsai, C. W., et al. 2013, *AJ*, 145, 6

Koleva, M., Prugniel, P., de Rijcke, S., & Zeilinger, W. W. 2011, *MNRAS*, 417, 1643

Kotulla, R., Fritze, U., Weilbacher, P., & Anders, P. 2009, *MNRAS*, 396, 462

Kuntschner, H., Emsellem, E., Bacon, R., et al. 2010, *MNRAS*, 408, 97

Ma, J., Fan, Z., de Grijs, R., et al. 2009, *AJ*, 137, 4884

Mainzer, A., Bauer, J., Grav, T., et al. 2011, *ApJ*, 731, 53

Maraston, C. 2005, *MNRAS*, 362, 799

Marigo, P., Girardi, L., Bressan, A., et al. 2008, *A&A*, 482, 883

McLaughlin, D. E., & van der Marel, R. P. 2005, *ApJS*, 161, 304

Meidt, S. E., Schinnerer, E., Knapen, J. H., et al. 2012, *ApJ*, 744, 17

Meidt, S. E., Schinnerer, E., van de Ven, G., et al. 2014, *ApJ*, 788, 144

Michielsen, D., Boselli, A., Conselice, C. J., et al. 2008, *MNRAS*, 385, 1374

Paturel, G., Petit, C., Prugniel, P., et al. 2003, *A&A*, 412, 45

Peletier, R. F., Kutdemir, E., van der Wolk, G., et al. 2012, *MNRAS*, 419, 2031

Popescu, B., & Hanson, M. M. 2010, *ApJ*, 724, 296

Ryś, A., Falcón-Barroso, J., & van de Ven, G. 2013, *MNRAS*, 428, 2980

Ryś, A., van de Ven, G., & Falcón-Barroso, J. 2014, *MNRAS*, 439, 284

Sheth, K., Regan, M., Hinz, J. L., et al. 2010, *PASP*, 122, 1397

Spitler, L. R., Forbes, D. A., & Beasley, M. A. 2008, *MNRAS*, 389, 1150

Thomas, D., Maraston, C., & Bender, R. 2003, *MNRAS*, 339, 897

Walcher, J., Groves, B., Budavári, T., & Dale, D. 2011, *Ap&SS*, 331, 1

Wang, S., Fan, Z., Ma, J., de Grijs, R., & Zhou, X. 2010, *AJ*, 139, 1438

Wright, E. L., Eisenhardt, P. R. M., Mainzer, A. K., et al. 2010, *AJ*, 140, 1868

Yuan, H. B., Liu, X. W., & Xiang, M. S. 2013, *MNRAS*, 430, 2188